k·p theory of semiconductor superlattice electronic structure. II. Application to $Ga_{1-x}In_xAs$-$Al_{1-y}In_yAs$ [100] superlattices

C. Mailhiot

Xerox Corporation, Webster Research Center, 800 Phillips Road (0114-41D), Webster, New York 14580

D. L. Smith

Los Alamos National Laboratory, University of California, Los Alamos, New Mexico 87545

(Received 27 January 1986)

This is the second of a two-paper series in which we present a complete k·p theory of semiconductor superlattices. In the first paper, the formal theoretical results are presented. Here, the numerical implementation of these results is described and they are used to investigate the electronic structure of $Ga_{1-x}In_xAs$-$Al_{1-y}In_yAs$ superlattices grown along the [100] direction. Three alloy composition pairs are considered: a lattice-matched case ($x = 0.53$, $y = 0.52$), a case where the Ga-containing layers are in biaxial tension with a 1% lattice mismatch ($x = 0.53$, $y = 0.67$) and a case where the Ga-containing layers are in biaxial compression with a 1% lattice mismatch ($x = 0.53$, $y = 0.37$). Our results for the superlattice energy band gap of the lattice-matched system are in good agreement with available experimental results. Calculations of subband energy dispersion for superlattice wave vectors both parallel and perpendicular to the growth axis are performed. These calculations show band-splitting and -mixing features not embodied within current envelope-function models which do not correctly describe the superlattice symmetry. However, these features are present in tight-binding models which do properly account for the superlattice symmetry. The origin of these band splitting and mixing features in the present k·p theory is discussed.

I. INTRODUCTION

The recent technical achievement of precisely controlled epitaxial-growth techniques has motivated detailed investigations of the electronic properties of layered structures formed by the alternating deposition of approximately lattice-matched semiconductors.[1] The inherent flexibility at tailoring the electronic band structure of these semiconductor superlattices according to controlled variations in the growth parameters is enhanced relative to that afforded by alloying. In addition to this tunability of the electronic band structure, the emergence of novel electronic and optical properties has led to intensive research activities focused on the potential use of such systems in various technological areas: semiconductor lasers,[2] detectors,[3] new transistor design,[4,5] etc.

The present study is concerned with the application of a new k·p theory of the electronic structure of semiconductor superlattices described in Ref. 6 (hereafter referred to as paper I). For illustrative purposes, we consider $Ga_{1-x}In_xAs$-$Al_{1-y}In_yAs$ superlattices grown along the [100] crystallographic axis. The motivation for studying this system lies in its potential application in the field of optical communications.[7] Moreover, $Ga_{1-x}In_xAs$-$Al_{1-y}In_yAs$ superlattices are currently being epitaxially grown on InP[100] substrates for an alloy composition which exhibits lattice matching with this substrate, i.e., $x=0.53$ and $y = 0.52$.[7-12] Thus, an opportunity exists for comparing our calculations with experimental measurements of parameters characterizing the electronic band structure of this system.

A description of the superlattice wave function is formulated in terms of a linear combination of propagating and evanescent bulk Bloch states of the constituent semiconductors. These bulk Bloch states are associated with complex values of the component of the crystal wave vector parallel to the superlattice growth axis. A single expansion set of zone-center basis functions, derived from a reference pseudopotential Hamiltonian, is used to describe the bulk Bloch states of the constituent semiconductors. Since the pseudopotentials associated with the constituent semiconductors are different, the zone-center eigenstates of the two materials are not identical and are therefore described by different linear combinations of the basis functions forming the expansion set. In previous models based on the k·p formalism,[13-16] the zone-center energy eigenstates of the two constituent materials were assumed to be the same. This assumption builds more symmetry into the model than the physical system actually has. As a result, energy band splitting and crossing features are not properly described. In our theory, the superlattice symmetry is correctly accounted for. Moreover, good correspondence is found between our results and experiments performed on $Ga_{1-x}In_xAs$-$Al_{1-y}In_yAs$ superlattices.

For alloy compositions such that only approximate lattice matching at the superlattice interfaces is realized, the effects of the resulting internal strain on the superlattice electronic band structure are also investigated. This is accomplished by extending our model to encompass a description of the bulk band structure of each constituent semiconductor under the influence of a lattice-mismatch-induced internal strain.

The paper is organized as follows: In Sec. II we

TABLE I. Symmetric and antisymmetric empirical pseudo-potential form factors. $V^S(G)$ and $V^A(G)$, respectively, for GaAs, AlAs, and InAs. Energy units are eV and the modulus of the reciprocal-lattice vector, $G \equiv |G|$, is in units of $2\pi/a_0$, where a_0 is the bulk lattice constant and is also indicated for GaAs, AlAs, and InAs.

	GaAs	AlAs	InAs
$V^S(\sqrt{3})$	-3.13	-2.99	-2.99
$V^S(\sqrt{4})$	0	0	0
$V^S(\sqrt{8})$	0.14	0.41	0
$V^S(\sqrt{11})$	0.83	0.92	0.69
$V^A(\sqrt{3})$	0.95	0.99	1.09
$V^A(\sqrt{4})$	0.68	0.85	0.68
$V^A(\sqrt{8})$	0	0	0
$V^A(\sqrt{11})$	0.14	-0.10	0.41
a_0 (Å)	5.653 15	5.6622	6.058 38

describe the numerical implementation of the general k·p theory described in paper I. Detailed numerical calculations for $Ga_{1-x}In_xAs$-$Al_{1-y}In_yAs$ superlattices are presented in Sec. III and compared with available experimental data. We conclude with a synopsis in Sec. IV.

II. ELECTRONIC-STRUCTURE CALCULATION

The purpose of this section is to indicate the computational procedure used for the calculation of the electronic structure of semiconductor superlattices within the framework of the k·p theory discussed in paper I. We proceed by first describing the empirical pseudopotential model which serves as the basis for the calculation of the bulk electronic structure of the constituent semiconductors.

We then examine how the bulk k·p Hamiltonian of each semiconductor is obtained from this pseudopotential description. We give the empirical parameters used in the calculation and describe propagating and evanescent bulk Bloch solutions for fixed energy and component of the wave vector parallel to the interface, $k_{\parallel}$. Methods to solve the superlattice eigenvalue problem are then presented.

The single basis set used to describe cell-periodic functions[17] of each semiconductor is derived from a reference pseudopotential Hamiltonian constructed by averaging the pseudopotentials of the constituent materials [Eq. (1) of paper I]. The empirical pseudopotential approach of Ref. 18 is used. In the present application, we describe the bulk electronic structure of the alloys $Ga_{1-x}In_xAs$ and $Al_{1-y}In_yAs$. We use a virtual-crystal approximation and perform the following weighted average of the pseudopotential form factors:[19]

$$V^{(l)}(G) = \frac{1}{\Omega(A^l_{1-x}B^l_x)}[(1-x)\Omega(A^l)V^{(l)}_A(G)$$

$$+ x\Omega(B^l)V^{(l)}_B(G)], \tag{1}$$

where $A^l \equiv GaAs$, $B^l \equiv InAs$ for the alloy $Ga_{1-x}In_xAs$, and $A^l \equiv AlAs$, $B^l \equiv InAs$ for the alloy $Al_{1-y}In_yAs$. In Eq. (1), the terms $\Omega(A)$, $\Omega(B)$, and $\Omega(A_{1-x}B_x)$ represent the volumes of the unit cell of semiconductors A,B, and of the alloy $A_{1-x}B_x$, respectively. Empirical pseudopotential form factors which provide a good description of the bulk electronic band structure of GaAs, AlAs, and InAs are indicated in Table I. These form factors are extracted from Refs. 18 and 20 and are modified by varying the symmetric form factor $V^S(G=\sqrt{11})$ to yield good agreement with low-temperature direct-energy-band-gap values. We use a set of 113 plane waves in the expansion

TABLE II. Numerical values (in Rydberg atomic units) of various matrix elements used in the evaluation of the bulk Hamiltonian and current-density matrices for $Ga_{1-x}In_xAs$-$Al_{1-y}In_yAs$ superlattices. The matrix elements are defined in Appendix I of paper I and are evaluated using the zone-center energy eigenstates and eigenvalues of the reference Hamiltonian. Energy band gaps are expressed in eV.

	$x = 0.53$ $y = 0.52$	$x = 0.53$ $y = 0.67$	$x = 0.53$ $y = 0.37$
A'	-5.17×10^{-2}	-5.48×10^{-2}	-4.84×10^{-2}
B	4.48×10^{-2}	4.89×10^{-2}	4.33×10^{-2}
P	1.10	1.09	1.10
L'	-1.40	-1.39	-1.41
M	-2.92	-2.89	-2.95
N'	-1.80	-1.76	-1.84
$\Delta\varepsilon_s^{(1)}$	-2.26×10^{-2}	-1.14×10^{-2}	-3.46×10^{-2}
$\Delta\varepsilon_p^{(1)}$	3.85×10^{-3}	6.94×10^{-4}	7.27×10^{-3}
$\Delta P^{(1)}$	2.48×10^{-3}	-4.80×10^{-5}	4.69×10^{-3}
$i\Delta_{SZ}$	1.38×10^{-3}	6.28×10^{-4}	2.06×10^{-3}
$i\Delta_{ZS}$	-6.34×10^{-3}	-5.32×10^{-4}	-1.14×10^{-2}
$i\Delta_{xy}$	-1.65×10^{-2}	-1.34×10^{-2}	-2.02×10^{-2}
$E_g(Ga_{1-x}In_xAs)$	0.79	0.79	0.79
$E_g(Al_{1-y}In_yAs)$	1.52	1.12	1.94

for the cell-periodic basis functions [Eq. (2) of paper I]. The cell-periodic functions are taken to be real, orthonormal, and to transform according to standard irreducible-representation conventions.[21]

From the zone-center energy eigenvalues and eigenvectors, the **k·p** momentum matrix elements, as defined in Appendixes A and B of paper I, are calculated. For this calculation we retain the 27 lowest-energy zone-center eigenstates. The Γ_{15} valence-band states and the Γ_1 conduction-band state are combined with a spinor and treated explicitly. Moreover, the 23 zone-center states nearest in energy are included in Löwdin perturbation theory[22] and are used to calculate the **k·p** momentum matrix elements.[23] Results applicable to the system $Ga_{1-x}In_xAs$-$Al_{1-y}In_yAs$ are shown in Table II. We explicitly consider three alloy composition pairs (x,y) for which the constituent alloys have a direct energy gap occurring at the center of the bulk Brillouin zone. In paper I, 16- and 12-band superlattice models are described. The 12-band model is obtained by setting the second-order matrix elements A' and L' equal to -1 a.u. in Table II.

Empirical parameters describing the stress Hamiltonian[24-26] (deformation-potential constants and elastic constants) and the spin-orbit Hamiltonian[27] are listed in Table III. The deformation potentials and elastic constants of AlAs are unknown and we have set them equal to GaAs values. The virtual-crystal approximation is used to obtain the deformation potentials, elastic constants, spin-orbit splittings, and lattice constants for the alloys from a knowledge of the corresponding quantities in GaAs, AlAs, and InAs.

The energy lineup (energy band offset) constitutes an empirical input to our model and is extracted from recent current-voltage—profiling measurements on $Ga_{1-x}In_xAs$-$Al_{1-y}In_yAs$ heterojunctions[7] at the lattice-matched alloy composition, $x = 0.53$ and $y = 0.52$. This work shows that the ratio of the conduction-band offset (ΔE_g) to the difference in band gap between $Ga_{0.47}In_{0.53}As$ and $Al_{0.48}In_{0.52}As$ (ΔE_g) is of the order of 0.71 ± 0.07. For the present purposes, a value of $\Delta E_v = \Delta E_g - \Delta E_c = 0.315 \Delta E_g$ was adopted for the magnitude of the valence-band offset for all alloy compositions studied. In the determination of ΔE_v, the quantity ΔE_g represents the band-gap difference between the unstressed

alloys. The valence-band maximum of $Ga_{1-x}In_xAs$ is raised by an energy ΔE_v relative to the valence-band maximum of $Al_{1-y}In_yAs$. The deformation potentials have been taken so that $l + 2m = 0$ in each material. This choice fixes the "center of mass" of the zone-center valence-band states under the effect of the applied stress. It is a prescription for treating stress dependence of the valence-band offset.[28] The zero of energy is chosen to be the valence-band maximum in the unstressed $Ga_{0.47}In_{0.53}As$ alloy.

From the calculated **k·p** momentum matrix elements and the various empirical inputs discussed above, bulk Hamiltonians for the two materials are constructed. For these calculations the 12-band model described in Sec. II of paper I is adopted. We solve [paper I, Eq. (12)] for the bulk eigenvectors and eigenvalues k (component of the bulk wave vector normal to the interface). The propagating and evanescent bulk Bloch states of the two materials are expanded in terms of a single basis of cell-periodic functions. The expansion amplitudes are normalized for each eigenvalue k_j so that

$$\sum_d (C_{dj}^l{}^*)^* C_{dj}^l = 1,$$ (2)

where the expansion coefficients C^l are defined by Eq. (5) of paper I. We adopt a phase convention such that the coefficient $C_{d_0j}^l$ is real for the component d_0 for which C_{dj}^l has a maximum modulus. In zinc-blende-structure compound semiconductors, symmetry-induced degeneracies (two energy eigenstates with identical k's) occur only for **k** along a [100] or [111] direction. If the **k·p** momentum matrix element B vanished, as occurs in the diamond structure,[23] a twofold degeneracy occurs at each **k** point throughout the bulk Brillouin zone. Degenerate states are orthogonalized, in the sense of Eq. (22) of paper I.

From a knowledge of the bulk Bloch eigenstates in the two materials, the current-density matrices are constructed in the fashion indicated in Appendix B of paper I. The superlattice eigenvalue equation has the form

$$\sum_{j'} M_{jj'} A_{j'\eta} = \exp[iQ_\eta(a+b)] A_{j\eta},$$ (3a)

where

$$M_{jj'} \equiv \exp(ik_j^a a) \frac{1}{J_{j*j}^a} \sum_i J_{j*i}^{ab} \exp(ik_i^b b) \frac{1}{J_{i*i}^b} J_{i*j'}^{ba},$$ (3b)

and a (b) is the thickness of semiconductor a (b) within the superlattice unit cell. Solution of Eqs. (3) yields the complex superlattice band structure. In many cases one is only interested in real superlattice wave vectors. In this case, it is numerically more convenient to rewrite the superlattice eigenvalue problem in the trigonometric form

$$[(M - J^{-1}\widetilde{M}J)/2i]_{jj'} A_{j'\eta} = \sin[Q_\eta(a+b)] A_{j\eta},$$ (4)

where the adjoint operation indicated by an overtilde is defined by Eq. (62) of paper I. For real superlattice band structure, a real wave vector Q_η is input and the matrix

$$F \equiv [(M - J^{-1}\widetilde{M}J)/2i] - \sin[Q_\eta(a+b)]\mathbb{1}$$ (5)

is constructed. The eigenvalues of the matrix F are found

TABLE III. Numerical values of deformation potentials (c,m,l), elastic constants (C_{11}, C_{12}), and spin-orbit splitings (Δ) for the alloys $Ga_{1-x}In_xAs$ and $Al_{1-y}In_yAs$. The notation adopted here is consistent with that used in Appendix A of paper I.

	Ga_1In_xAs	$Al_{1-y}In_yAs$
C_{11} (10^{11} dyn cm^{-2})	$11.81(1-x)+8.33x$	
C_{12} (10^{11} dyn cm^{-2})	$5.32(1-x)+4.53x$	
$-c$ (eV)	$8.23(1-x)+5.80x$	
m (eV)	1.70	
$-l$ (eV)	3.40	
Δ (eV)	$0.34(1-x)+.38x$	$0.28(1-y)+0.38y$

as a function of energy for fixed wavevector $\mathbf{k}_{||}$. Solutions to the eigenvalue equation [Eqs. (3)] for an input wave vector occur when F has a zero eigenvalue. For all energies and $\mathbf{k}_{||}$, the matrix F has a real determinant and the eigenvalues of F come in complex-conjugated pairs when Q_η is real. As a result, zeros in the eigenvalues of F are easily located numerically as a function of energy. For this reason the trigonometric form of the eigenvalue equation [Eq. (4)] is used when only real superlattice bands are of interest. The superlattice wave functions, expressed in terms of the bulk Bloch eigenstates of the two constituent semiconductors, are found from the eigenvectors of the matrix M (or equivalently F) and from the interface-matching condition [Eq. (30) of paper I].

In constructing the matrix M in Eq. (3b), factors of the form $\exp(ik_j^a a)$ appear. For bulk evanescent states, k_j is complex and such exponential factors can be very large or very small. It is difficult to handle such factors numerically. This problem is more acute for superlattices with a large unit cell. In the Appendix we describe the physical origin of this numerical problem and discuss its solution.

The main difference between the 16- and 12-band models lies in the presence of four bulk states with large imaginary parts of k. In the Appendix we show that such states modify the matrix M [Eqs. (3)] by terms of the form $(J_{p\ast l}^{ab}/J_{p\ast p}^{a})^2$, where p labels the physically significant states, l labels the large $\text{Im}[k]$ evanescent states which are not physically significant, and J refers to matrix elements of the current-density operator defined in paper I. Numerical calculations show these terms to be typically of order 10^{-6}. Thus, the 12- and 16-band models give essentially identical results.

III. APPLICATION TO $Ga_{1-x}In_xAs$-$Al_{1-y}In_yAs$ SUPERLATTICES

In this section we apply the theoretical formalism described in paper I to a detailed study of $Ga_{1-x}In_xAs$-$Al_{1-y}In_yAs$ superlattices epitaxially grown along the [100] crystallographic direction. Specifically, we consider three alloy composition pairs (x,y): one for which the system is lattice-matched to an InP[100] substrate $(x=0.53, y=0.52)$, one for which the interfacial lattice mismatch is $\Delta a_0/a_0 = 1\%$ $(x=0.53, y=0.67)$, and one for which the interfacial lattice mismatch is $\Delta a_0/a_0 = -1\%$ $(x=0.53, y=0.37)$, where

$$\Delta a_0/a_0 \equiv [a_0(Al_{1-y}In_yAs)$$
$$- a_0(Ga_{1-x}In_xAs)]/a_0(Ga_{1-x}In_xAs)$$

and a_0 is the bulk lattice constant of the alloy. We first discuss the lattice-matched system and then generalize the discussion to the lattice-mismatched cases.

A. Lattice-matched superlattices

The basic features governing the electronic structure of semiconductor superlattices are determined by two physical effects: (1) the spatial confinement of electrons and holes, and (2) the resulting quantization of their single-particle energy eigenvalue spectrum.[29] The quantitative

details of this electronic structure depend, however, on the nature of the model used to describe the bulk band structure of the constituent semiconductors and on the form of the interfacial boundary conditions imposed on the superlattice solutions. In the case of $Ga_{1-x}In_xAs$-$Al_{1-y}In_yAs$ superlattices, the energy band alignment is such that both electrons and holes are spatially confined within the (smaller-band-gap) $Ga_{1-x}In_xAs$ layers. The single-particle energy eigenvalue spectrum of the superlattice solutions takes the form of a series of quantized subbands whose dispersion relations are sensitive functions of the superlattice growth parameters (layer thickness, alloy composition, etc.).

We now examine the dependence of the subband energy levels as a function of the size of the superlattice unit cell. Figure 1 displays the superlattice energy gap (it occurs at the center of the Brillouin zone) as a function of the total number of layers in the superlattice unit cell for three ratios

$$r \equiv N_b(Al_{0.48}In_{0.52}As)/M_a(Ga_{0.47}In_{0.53}As),$$

where M_a (N_b) is the number of monolayers of the semiconductor a (b) within the superlattice primitive cell. Hereafter, the label a (b) refers to the alloy $Ga_{1-x}In_xAs$-$Al_{1-y}In_yAs$). As is clearly demonstrated in Fig. 1, it is possible to adjust the superlattice band gap, for fixed superlattice period, by modifying the thickness of one constituent semiconductor relative to that of the other. This flexibility at varying the superlattice energy gap with layer thickness is well documented.[30] As the thickness of the smaller-band-gap material is increased, for fixed total layer thickness, the superlattice band gap decreases. This occurs because the wells in which the carriers are confined
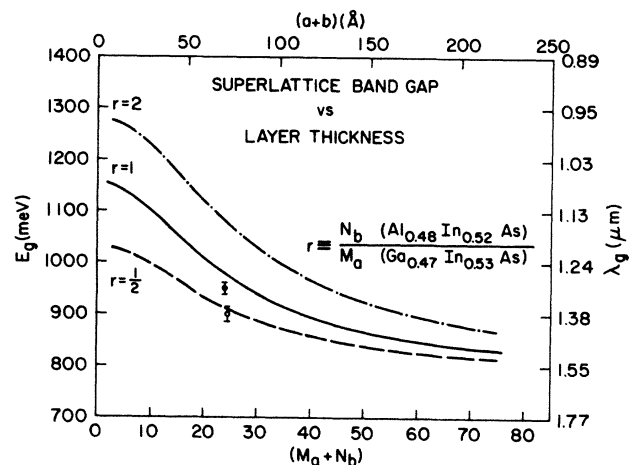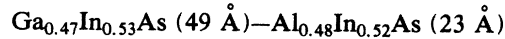

FIG. 1. Superlattice energy gap plotted as a function of the total number of monolayers $(M_a + N_b)$ contained within the superlattice primitive cell for three ratios $N_b(Al_{0.48}In_{0.52}As)/M_a(Ga_{0.47}In_{0.53}As)$. For superlattices grown along the [100] orientation, the thickness of a monolayer in material a (b) is $a_0/2$, where a_0 is the bulk lattice constant of the alloy a (b). Experimental points are from Refs. 8 (●) and 9 (○). The wavelength λ_g is defined as $E_g = 2\pi\hbar c/\lambda_g$.

increases in size. For fixed r, the superlattice energy gap E_g is a monotonically decreasing function of the total length of the superlattice period as indicated by Fig. 1. As the size of the superlattice period is increased, the conduction-subband level approaches the conduction-band minimum of $Ga_{0.47}In_{0.53}As$, whereas the heavy-hole subband level approaches the maximum of the valence band of the same alloy. The net effect is a reduction in the band gap. Also shown in Fig. 1 is the measured energy gap of a

$Ga_{0.47}In_{0.53}As$ (35 Å)—$Al_{0.48}In_{0.52}As$ (35 Å)
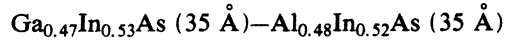
($r=1$) (Ref. 8) superlattice and a

$Ga_{0.47}In_{0.53}As$ (49 Å)—$Al_{0.48}In_{0.52}As$ (23 Å)

($r \sim \frac{1}{2}$) (Ref. 9) superlattice as extracted from recent photocurrent responsivity measurements. Examination of Fig. 1 shows that a good correspondence exists between our calculations and experimental observations of superlattice energy band gaps.

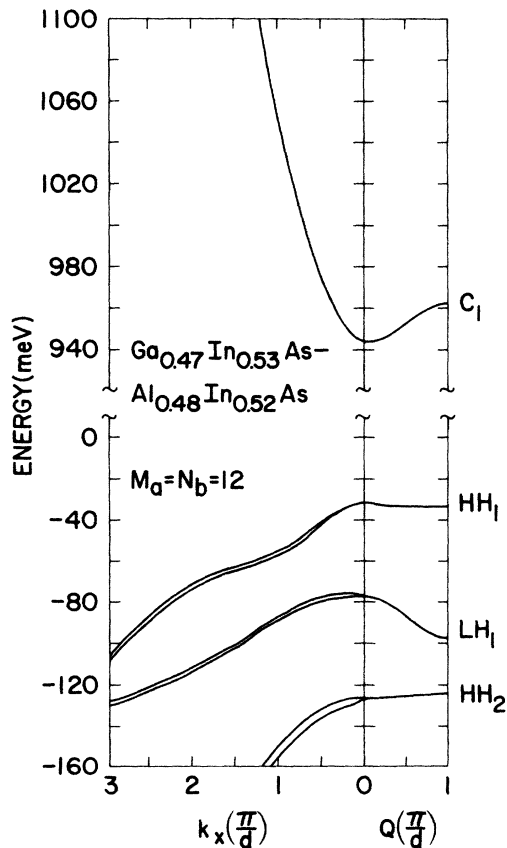We now examine the subband energy dispersion of

FIG. 2. Electronic energy band structure of a superlattice consisting of 12 layers of $Ga_{0.47}In_{0.53}As$ alternating with 12 layers of $Al_{0.48}In_{0.52}As$. The superlattice wave vector is defined as $Q \equiv k_{||} + \hat{z}Q$ with $k_{||} = \hat{x}k_x + \hat{y}k_y$ and $\hat{z}$ oriented along the superlattice growth axis. The energy zero coincides with the valence-band maximum of the $Ga_{0.47}In_{0.53}As$ alloy.
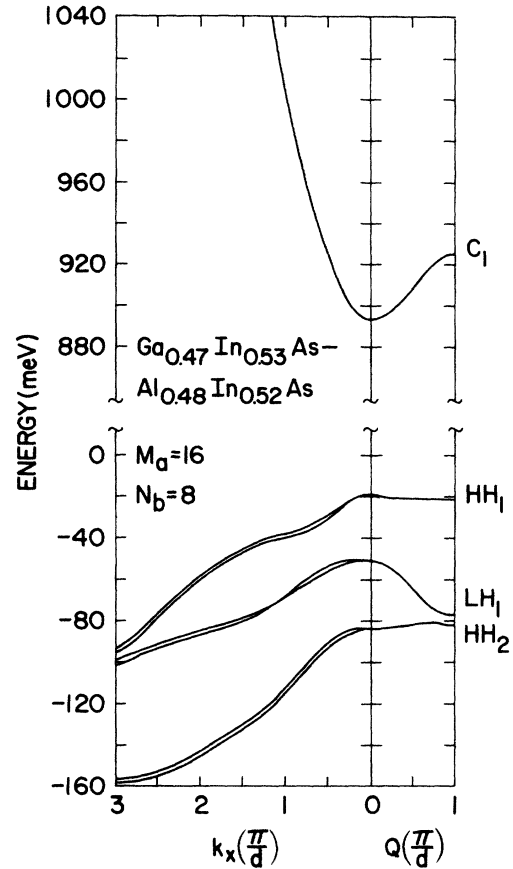

FIG. 3. Electronic energy band structure of a superlattice consisting of 16 layers of $Ga_{0.47}In_{0.53}As$ alternating with eight layers of $Al_{0.48}In_{0.52}As$. The superlattice wave vector is defined as $Q \equiv k_{||} + \hat{z}Q$ with $k_{||} = \hat{x}k_x + \hat{y}k_y$ and $\hat{z}$ oriented along the superlattice growth axis. The energy zero coincides with the valence-band maximum of the $Ga_{0.47}In_{0.53}As$ alloy.

$Ga_{0.47}In_{0.53}As$-$Al_{0.48}In_{0.52}As$ superlattices for wave vectors parallel to the [100] growth axis ($k_{||} = 0$) or perpendicular to it ($k_{||} = \hat{x}k_x$). We consider the cases $M_a/N_b = 12/12$ and 16/8, which correspond approximately to the experimental situations described in Refs. 8 and 9, respectively. The electronic band structures for the lowest-lying conduction and a few valence superlattice subbands are shown in Figs. 2 and 3. In the discussion hereafter, we refer to superlattice states by labeling them according to their dominant bulk-state component: conduction (C_n), heavy-hole (HH_n), light-hole (LH_n), or spin-split-off hole (SOH_n), where n orders the states by increasing energy.

At the center of the Brillouin zone, four twofold-degenerate pairs[31] of states are shown. These states are labeled C_1, HH_1, LH_1, and HH_2 in order of decreasing energy. In Table IV the relative admixture of the bulk eigenstates in the superlattice wave function for the four pairs of states are shown for the $M_a/N_b = 12/12$ case. The labeling of the superlattice solutions is clearly unambiguous. The energies reported here for the subbands C_1 and HH_1 are compatible with those extracted from an effective-mass model extended to include band nonpara-

TABLE IV. Relative admixture, in percent, of various bulk states in the superlattice wave functions at the center of the Brillouin zone. The bulk state components are labeled by C-LH (conduction—light hole), HH (heavy hole), and SOH (spin-split-off hole). The superlattice consists of 12 layers (35 Å) of $Ga_{0.47}In_{0.53}As$ alternating with 12 layers (35 Å) of $Al_{0.48}In_{0.52}As$. For each energy, the top (bottom) entry refers to the admixtures in the superlattice wave function localized within the $Ga_{0.47}In_{0.53}As$ ($Al_{0.48}In_{0.52}As$) layers.

Energy (meV)	C-LH	HH	SOH
−126	1	97	2
	2	95	3
−78	86	2	12
	77	7	16
−33	3	96	1
	4	93	3
944	99.1	0.03	0.87
	99.3	0.3	0.4

bolicity effects.[8,9,32]

As Q increases from zero, the conduction and light-hole bands show appreciable dispersion, whereas the heavy-hole bands are fairly dispersionless. There is an exception in the $M_a/N_b = 16/8$ case for the HH_2 band near the superlattice Brillouin-zone edge. In this case, strong hybridization between the HH_2 and LH_1 superlattice bands occurs. For superlattice wave vector parallel to the [100] growth axis ($k_{||} = 0$), the small point group is C_{2v}. The double group contains a single two-dimensional representation[21] and all subbands are double degenerate. Since all superlattice solutions belong to the same double degenerate representation, crossing of the subbands is forbidden as a function of Q for $K_{||} = 0$.[33] The k·p theory presented here correctly describes the symmetry of the physical system and thus does not allow band crossing in this direction. The mixing of heavy-hole- and light-hole-like states originates from the difference-potential terms (ΔV) in the current-density matrices J^{ab} and J^{ba} (i.e., the matrices $\Delta_{dd'}$ in Appendix B of paper I) which enter in the interfacial boundary conditions. If the zone-center states in the two constituent materials are assumed to be the same,[13–16] this mixing does not occur.

We now examine the subband dispersion for superlattice wave vector oriented perpendicular to the superlattice [100] growth axis, i.e., $k_{||} = \hat{x}k_x$ and $Q = 0$. A detailed knowledge of the subband dispersion relation in the plane of the layers is of considerable interest with regard to the calculation of density of states, optical absorption,[34,35] transport properties, motion of carriers in an externally applied magnetic field,[36] etc. Degeneracies are lifted for all the bands. In all cases the band splitting is small. For the conduction band the energy splitting is too small to be resolved on the energy scale used here. At small $|k_x|$, the heavy-hole subbands show somewhat larger dispersion than the light-hole subbands in the direction parallel to the superlattice layers. At larger $|k_x|$, the heavy- and

light-hole subbands hybridize. For superlattice wave vectors in this direction, the little group is C_2. In the limit of very large periods, so that the layers have the characteristics of the corresponding bulk material, the little group is extended to C_{2v}. C_2 has two one-dimensional representations compatible with spin.[21] These two representations are also compatible with the single two-dimensional representation of the C_{2v} double group.[21] The band splitting occurs because of the reduction in symmetry in going from the bulk materials to the superlattice structure.[33] It decreases as the layer thickness of the smaller-gap materials increases. If the III-V compounds considered here were replaced with group-IV compounds (necessarily even numbers of group-IV atomic layers), the superlattice would have inversion symmetry. In this case a combination of inversion and time-reversal symmetry would ensure a twofold degeneracy of the bands everywhere in the superlattice Brillouin zone. In k·p theory, the difference between the symmetry of the group-III-V and -IV materials appears in the k·p momentum matrix element B which is zero in group-IV materials.[23] k·p models in which the parameter B does not appear[16,37] will not show the energy band splittings observed in Figs. 2 and 3.

The valence-band energy splitting at the center of the superlattice Brillouin zone is produced by the spatial confinement of the states in the smaller-band-gap $Ga_{0.47}In_{0.53}As$. Because this confinement is in the $\hat{z}$ direction, the zone-center states are well separated into heavy- and light-hole states, where heavy and light hole refer to k and $\hat{z}$ (growth axis) direction. However, when k is in the $\hat{x}$ direction, the zone-center states are mixed combinations of "$\hat{x}$-direction heavy- and light-hole" states.[37,38] Indeed, by considering spin-3/2 rotation matrices one finds that the HH states have a larger "x-direction light-hole" amplitude than the LH states by a factor of $\sqrt{3}$. This accounts for their greater dispersion at small $|k_x|$. At larger $|k_x|$, there is strong mixing and hybridization between these bands, leading to complex and very nonparabolic dispersion.[33,37] The symmetry of these bands is the same even when perturbation terms in ΔV are neglected. Thus, the mixing between them is strong.

The squared envelope functions[39] of the four zone-center states for the $M_a/N_b = 12/12$ superlattice are shown as a function of position for one superlattice cycle in Fig. 4. The nodal structure of these envelope functions shows the particle-in-a-well nature of the superlattice solutions. The HH states have equal $|x\rangle$ and $|y\rangle$ components and virtually no $|s\rangle$ or $|z\rangle$ components.[40] The C_1 state has primarily a $|s\rangle$ component with some $|z\rangle$ and small amounts of $|x\rangle$ and $|y\rangle$ components (not shown) mixed in. The LH_1 state has primarily a $|z\rangle$ component with lesser amounts of $|x\rangle$, $|y\rangle$, and $|s\rangle$. The interface-matching conditions described in paper I ensure envelope-function continuity to zeroth order in the ΔV perturbation. For the 16-band model the envelope-function derivatives are also continuous to zeroth order in the ΔV perturbation term. However, in the 12-band model used in these calculations there are no conditions on the continuity of the envelope-function derivatives.[41] But from Fig. 4, one sees that both the envelope functions

and their normal derivatives are continuous to very good approximation.

B. Lattice-mismatched superlattices

In this subsection we consider situations corresponding to $Ga_{1-x}In_xAs-Al_{1-y}In_yAs$ superlattices for which im-

perfect lattice matching occurs at the superlattice interfaces. For sufficiently thin layers, the lattice mismatch is accommodated by internal strains rather than by the generation of dislocations.[42] Although the effects of lattice-mismatch-induced internal strain on the electronic structure of semiconductor superlattices are well documented,[43] extension of current models to lattice-mismatched
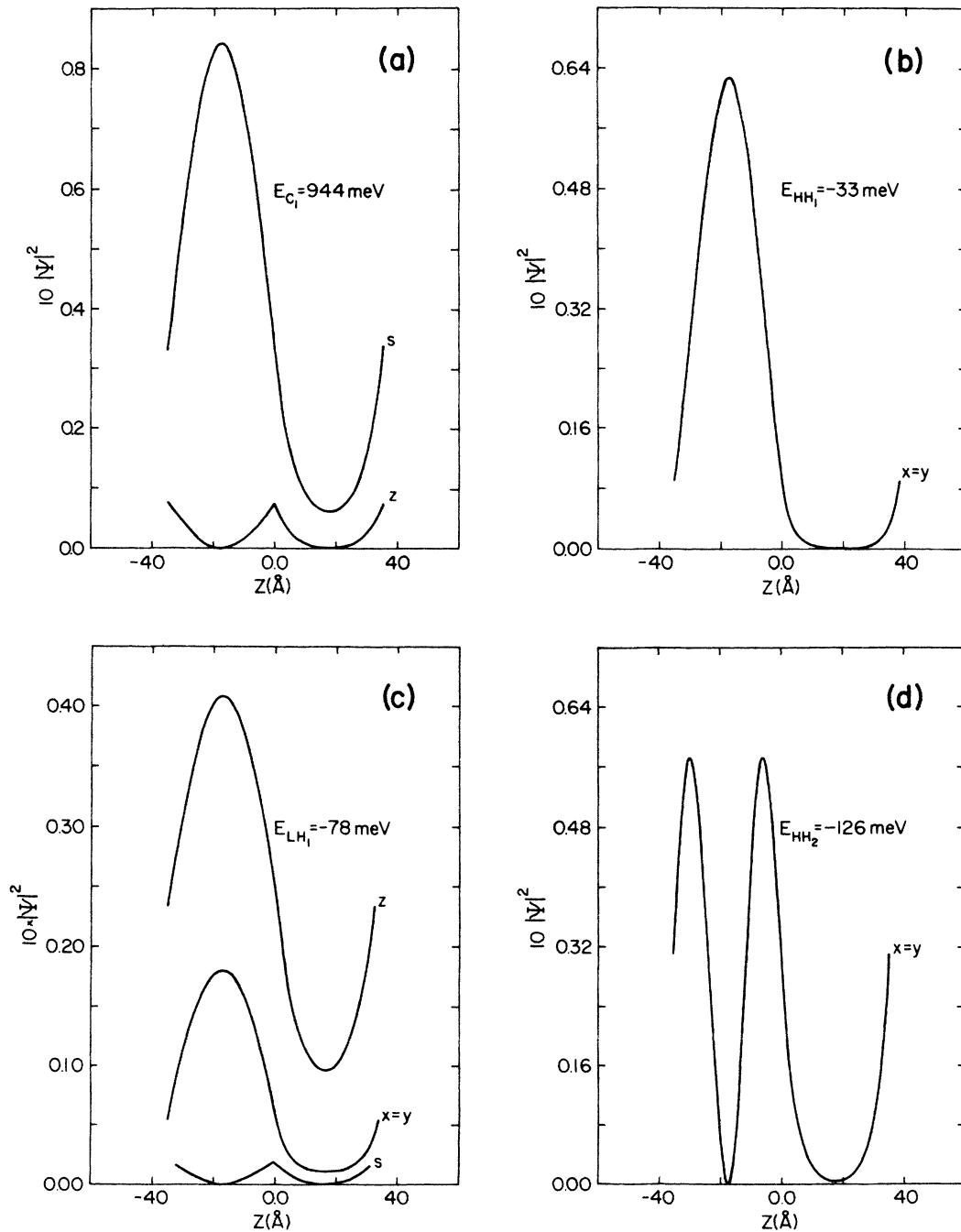
FIG. 4. Squared amplitude of symmetry-resolved envelope functions for a superlattice consisting of 12 layers of $Ga_{0.47}In_{0.53}As$ alternating with 12 layers of $Al_{0.48}In_{0.52}As$. The origin is taken at the $Ga_{0.47}In_{0.53}As/Al_{0.48}In_{0.52}As$ interface. The electronic band structure of this superlattice is shown in Fig. 2 with the corresponding labeling of the subbands.

$Ga_{1-x}In_xAs-Al_{1-y}In_yAs$ semiconductor superlattices has not yet been made.

We consider the cases where the alloy composition in $Ga_{1-x}In_xAs$ is kept fixed at the value $x=0.53$, whereas the alloy composition in $Al_{1-y}In_yAs$ is varied to produce a relative lattice mismatch of $\Delta a_0/a_0=1\%$ ($y=0.67$) and

$\Delta a_0/a_0=-1\%$ ($y=0.37$). For finite lattice mismatch, the material with the smaller lattice constant expands in the interface plane as a result of biaxial tensile stress, whereas the material with the larger lattice constant contracts in the interface plane due to a biaxial compressive stress of equal magnitude. For the material with the
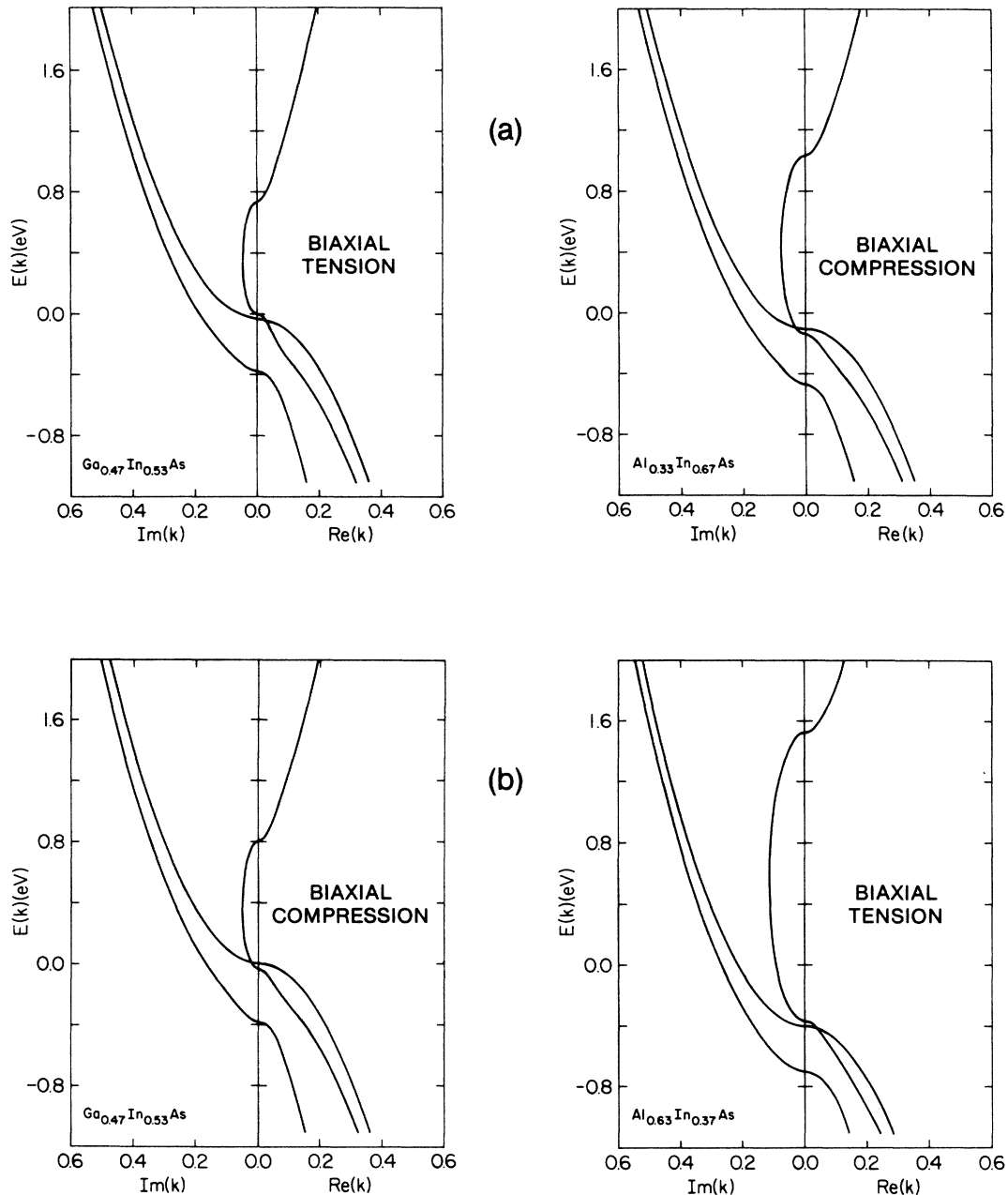
FIG. 5. Effect of biaxial stress on the complex-k bulk electronic structure of $Ga_{0.47}In_{0.53}As$ and $Al_{1-y}In_yAs$. The energy shift corresponding to the valence-band offset (ΔE_v) has been incorporated into the calculation. The zero of energy coincides with the maximum of the valence band of unstressed $Ga_{0.47}In_{0.53}As$. The strain is calculated for a superlattice consisting of 12 layers of $Ga_{0.47}In_{0.53}As$ alternating with 12 layers of $Al_{1-y}In_yAs$. The real and imaginary parts of k (component of the crystal wave vector parallel to the [100] growth axis) are in units of $2\pi/a_0$, where a_0 is the bulk lattice constant of the alloy. (a) For the alloy compositions $x=0.53$ and $y=0.67$, the $Ga_{0.47}In_{0.53}As$ layers are under biaxial tensile stress, whereas the $Al_{0.33}In_{0.67}As$ layers are under biaxial compressive stress due to a lattice mismatch $\Delta a_0/a_0=1\%$. (b) For the alloy compositions $x=0.53$ and $y=0.37$, the $Ga_{0.47}In_{0.53}As$ layers are under biaxial compressive stress, whereas the $Al_{0.63}In_{0.37}As$ layers are under biaxial tensile stress due to a lattice mismatch $\Delta a_0/a_0=-1\%$.

smaller (larger) lattice constant, this situation can be analyzed in terms of a combination of a hydrostatic dilation (compression) plus a uniaxial compression (dilation) along the superlattice [100] axis. The net result on the bulk electronic band structure is twofold: the hydrostatic dilation (compression) produces a decrease (increase) of the energy band gap, whereas the effect of a uniaxial compressive (tensile) stress is to lift the degeneracy of the fourfold valence-band at the center of the bulk Brillouin zone by lowering (raising) the heavy-hole state with respect to the light-hole state. The presence of a uniaxial compressive (tensile) stress also leads to an increase (decrease) of the band gap.

In a superlattice system, the magnitude of the strain is related to the layer thickness of each material, the thinner of the two materials having the greater internal strain.[43] Explicit formulas applicable to the case of [100]-growth-axis superlattices are given in Appendix A of paper I. The effects of stress on the bulk electronic band structure of the alloys $Ga_{0.47}In_{0.53}As$ and $Al_{1-y}In_yAs$ are illustrated in Fig. 5 for different compositions y corresponding to lattice mismatches of magnitude $\Delta a_0/a_0 = 1\%$ [panel (a)]
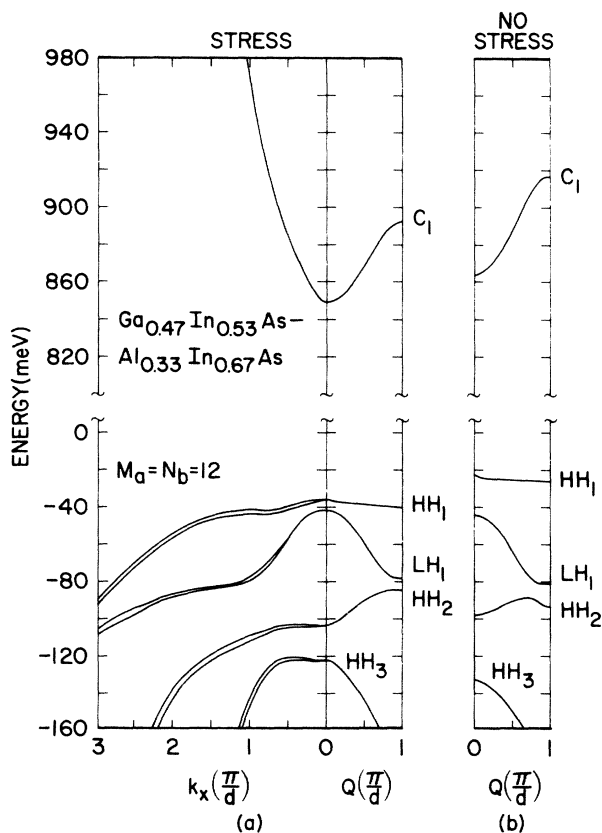

FIG. 6. Electronic energy band structure of a $\Delta a_0/a_0 = 1\%$ lattice-mismatched superlattice consisting of 12 layers of $Ga_{0.47}In_{0.53}As$ alternating with 12 layers of $Al_{0.33}In_{0.67}As$. The superlattice wave vector is defined as $Q \equiv k_{||} + \hat{z}Q$ with $k_{||} = \hat{x}k_x + \hat{y}k_y$ and $\hat{z}$ oriented along the superlattice growth axis. The energy zero coincides with the valence-band maximum of the (unstrained $Ga_{0.47}In_{0.53}As$ alloy. (a) Stress effects included. (b) Stress effects not included.
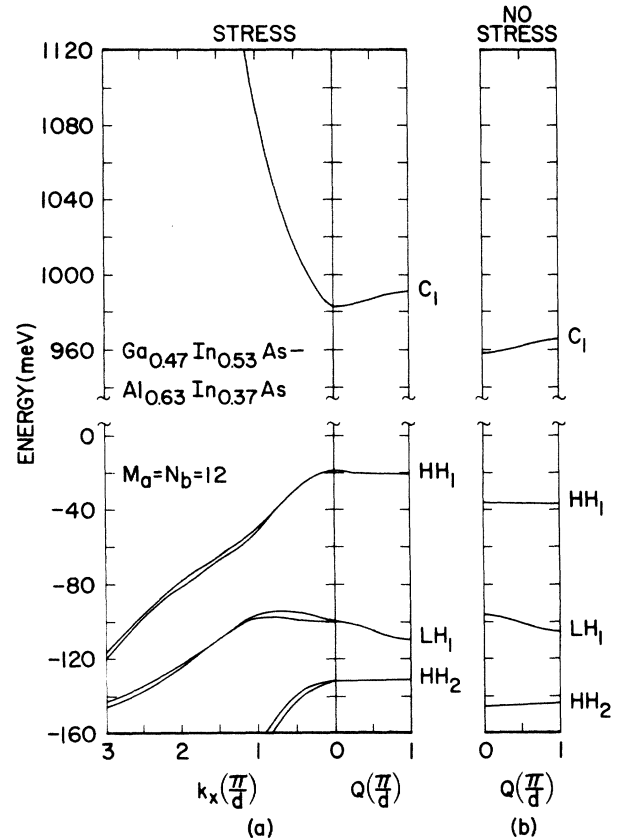

FIG. 7. Electronic energy band structure of a $\Delta a_0/a_0 = -1\%$ lattice-mismatched superlattice consisting of 12 layers of $Ga_{0.47}In_{0.53}As$ alternating with 12 layers of $Al_{0.63}In_{0.37}As$. The superlattice wave vector is defined as $Q \equiv k_{||} + \hat{z}Q$ with $k_{||} = \hat{x}k_x + \hat{y}k_y$ and $\hat{z}$ oriented along the superlattice growth axis. The energy zero coincides with the valence-band maximum of the (unstrained) $Ga_{0.47}In_{0.53}As$ alloy. (a) Stress effects included. (b) Stress effects not included.

and $\Delta a_0/a_0 = -1\%$ [panel (b)]. The strain is calculated for an $M_a/N_b = 12/12$ superlattice.

Electronic band structures of $Ga_{0.47}In_{0.53}As$ (35 Å)–$Al_{1-y}In_yAs$ (35 Å) strained-layer superlattices are shown in panel (a) of Figs. 6 and 7 for $y=0.67$ ($\Delta a_0/a_0 = 1\%$) and $y=0.37$ ($\Delta a_0/a_0 = -1\%$), respectively. The presence of a uniaxial stress can induce a reversal in the ordering of the superlattice subbands HH_1 and LH_1 by lowering the first heavy-hole subband (HH_1) below the first light-hole subband (LH_1).[44] However, for the cases illustrated by Figs. 6 and 7, such a reversal is not observed. The $k_{||} = 0$ portion of the band structure, in the case where stress-induced effects are neglected, is also shown in panel (b) of Figs. 6 and 7. Comparison between panels (a) and (b) of Figs. 6 and 7 shows the significance of including stress-induced effects in the description of the electronic band structure of semiconductor superlattices. In Fig. 6, where the smaller-band-gap $Ga_{0.47}In_{0.53}As$ is under biaxial tension, the splitting between the HH_1 and LH_1 states is reduced compared to the case where stress is ignored. If higher-stress cases are

considered, a reversal in energy position of these states is found. In Fig. 7, where the smaller-band-gap $Ga_{0.47}In_{0.53}As$ is under biaxial compression, the splitting between the HH_1 and LH_1 states is increased by stress. The qualitative features of the electronic band structure discussed in Sec. III A are also observed for lattice-mismatch superlattices, as suggested by comparison of Figs. 2, 3, 6, and 7. The strong hybridization of the hole subbands for $k_{||} \neq 0$ results in strikingly nonparabolic subband dispersion and, in some instances, in a positive value of the in-layer hole effective mass at the center of the superlattice Brillouin zone.

IV. SYNOPSIS

This paper has two main purposes: to describe the numerical implementation of the formal results presented in paper I and to use these results to investigate the electronic structure of $Ga_{1-x}In_xAs$-$Al_{1-y}In_yAs$ superlattices grown along the [100] direction. A reference pseudopotential Hamiltonian is used to construct a basis set of zone-center states which is used in the description of all the superlattice constituents. The Γ_{15} valence-band states and the Γ_1 conduction-band state, determined from the reference Hamiltonian, are combined with a spinor and treated explicitly. Moreover, the 23 zone-center states nearest in energy are included in Löwdin perturbation theory.[22] The perturbation operator is $\hbar \mathbf{k} \cdot \mathbf{p}/m + \Delta V$, where ΔV is the difference between the pseudopotentials of one of the constituent semiconductors and that of the reference material. The perturbation is included through first order in wave functions and to second order in energies. Inclusion of the ΔV perturbation through these orders (to be contrasted with calculations to zeroth order in wave functions and to first order in energies) causes the description of the superlattice to have the correct symmetry and to produce correct energy band splittings. The k·p momentum matrix elements and the parameters which result from the ΔV perturbation are calculated using the zone-center energy eigenfunctions and eigenvalues of the reference Hamiltonian. Spin-orbit interaction parameters, stress-interaction parameters (for strained-layer superlattices), and the valence-band offset are included empirically. In many cases, some k·p momentum matrix elements are empirically known. It would be possible to include these empirically determined values, rather than computed values, into our formal structure and thereby save a step in the implementation of the theory. Not all of the parameters which appear in the theory are likely to be known empirically, however, and care must be taken to treat things consistently. One should ensure flux conservation at the interface, for example.[45]

We have used our formal results to investigate the electronic band structure of the $Ga_{1-x}In_xAs$-$Al_{1-y}In_yAs$ superlattice. We first considered the lattice-matched case ($x=0.53$ and $y=0.52$). Results for the band gap of this superlattice are in good agreement with available experimental results. Our analysis was extended to the study of $Ga_{1-x}In_xAs$-$Al_{1-y}In_yAs$ superlattices in a range of alloy compositions where lattice-mismatch-induced internal strain is present in the layers. Calculations of subband en-

ergy dispersion for superlattice wave vectors parallel and perpendicular to the growth axis were performed and revealed features not embodied within current envelope-function models which do not correctly describe the superlattice symmetry, but are present in tight-binding models which do correctly describe the superlattice symmetry.[33]

APPENDIX: TREATMENT OF LARGE-$|Im[k]|$ BULK BLOCH STATES

In the construction of the matrix M appearing in the superlattice eigenvalue equation [Eq. (3)], factors of the form $\exp(ik_j a)$ appear. For bulk evanescent states with large values of $|Im[k]|$, such factors can be extremely large or extremely small. It is difficult to handle such factors numerically. The problem is more acute for superlattices with large unit cell. In this appendix we describe the physical origin of such factors and show how to treat them analytically so that numerical difficulties associated with very large or very small numbers do not appear.

We start by writing our basic superlattice equations [Eqs. (57) and (60) of paper I] and also equivalent inverted forms [see Eqs. (31) of paper I],

$$A_j = \sum_i \frac{J_{j*i}^{ab}}{J_{j*j}^a} B_i, \tag{A1a}$$

$$B_i = \sum_j \frac{J_{i*j}^{ba}}{J_{i*i}^b} A_j, \tag{A1b}$$

$$A_j \exp[iQ(a+b)] = \sum_i \exp(ik_j^a a) \frac{J_{j*i}^{ab}}{J_{j*j}^a} \exp(ik_i^b b) B_i, \tag{A1c}$$

$$B_i \exp[-iQ(a+b)] = \sum_j \exp(-ik_i^b b) \frac{J_{i*j}^{ba}}{J_{i*i}^b} \exp(-ik_j^a a) A_j, \tag{A1d}$$

where $j(i)$ labels the Bloch propagating and evanescent states in material a (b) and A_j (B_i) is the amplitude of the jth (ith) bulk eigenstate in material a (b) in the zeroth-cycle superlattice wave function [see Eq. (50), paper I]. Equations (A1a) and (A1b) are equivalent and Eqs. (A1c) and (A1d) are equivalent. Combining nonequivalent sets of these equations gives the superlattice eigenvalue equation.

Equations (A1a) and (A1b) are derived by considering the interface containing the origin of coordinates. They

do not contain exponential factors and pose no numerical problems. Equations (A1c) and (A1d) are derived by considering the interfaces at $z = b$ and $z = -a$ and using superlattice periodicity. They contain the factors $\exp(ik_i^b b)B_i$ and $\exp(-ik_j^a a)A_j$, which can cause numerical problems. (We assume that there is no interest in solutions for which $|\text{Im}[Q]|$ is a large number.) Physically, the factors $\exp(ik_i^b b)B_i$ and $\exp(-ik_j^a a)A_j$ are the amplitudes of bulk periodic states at $z = b$ and $z = -a$, respectively, in the superlattice wave function. Thus they cannot be extremely large numbers. However, the factors $\exp(ik_i^b b)$ and $\exp(-ik_j^a)$ can be extremely large by themselves. The solution of the problem for B_i and A_j must be such that the amplitudes at $z = b$ and $z = -a$ are of, at most, modest size. Although this will indeed happen if the problem is solved exactly, numerical problems can arise in practice.

Recognizing the origin of the large factors, it becomes clear how to treat them. For the states with large exponentials, take $\exp(ik_i^b b)B_i$ and $\exp(-ik_j^a a)A_j$ as the unknown variables. Thus one relabels states by

$$j \rightarrow \begin{cases} j & \text{if } |\text{Im}[k_j^a]| \leq \gamma/a, \quad\quad\text{(A2a)} \\ \eta & \text{if } \text{Im}[k_j^a] > \gamma/a, \quad\quad\text{(A2b)} \\ \eta^* & \text{if } \text{Im}[k_j^a] < -\gamma/a, \quad\text{(A2c)} \end{cases}$$

and

$$i \rightarrow \begin{cases} i & \text{if } |\text{Im}[k_i^b]| \leq \gamma'/b, \quad\quad\text{(A2d)} \\ \xi & \text{if } \text{Im}[k_i^b] < -\gamma'/b, \quad\text{(A2e)} \\ \xi^* & \text{if } \text{Im}[k_i^b] > \gamma'/b. \quad\quad\text{(A2f)} \end{cases}$$

It may be convenient to take the parameters γ and γ' to be distinct. One then makes a variable change by

$$\alpha_j = A_j, \quad\quad\quad\text{(A3a)}$$

$$\alpha_{\eta^*} = A_{\eta^*}, \quad\quad\quad\text{(A3b)}$$

$$\alpha_\eta = \exp(-ik_\eta^a a)A_\eta, \quad\quad\text{(A3c)}$$

and

$$\beta_i = B_i, \quad\quad\quad\text{(A3d)}$$

$$\beta_{\xi^*} = B_{\xi^*}, \quad\quad\quad\text{(A3e)}$$

$$\beta_\xi = \exp(ik_\xi^b b)B_\xi. \quad\quad\text{(A3f)}$$

These variables are substituted into Eqs. (A1) and exponentially small terms are dropped. For example, substituting into Eq. (A1c) gives

$$\alpha_j \exp[iQ(a+b)] = \sum_i \exp(ik_j^a a)\frac{J_{j^*i}^{ab}}{J_{j^*j}^a}\exp(ik_i^b b)\beta_i$$

$$+ \sum_{\xi^*} \exp(ik_j^a a)\frac{J_{j^*\xi^*}^{ab}}{J_{j^*j}^a}\exp(ik_{\xi^*}^b b)\beta_{\xi^*}$$

$$+ \sum_\xi \exp(ik_j^a a)\frac{J_{j^*\xi}^{ab}}{J_{j^*j}^a}\beta_\xi, \quad\quad\text{(A4a)}$$

$$\alpha_{\eta^*}\exp[iQ(a+b)]$$

$$= \exp(ik_{\eta^*}^a a)\left[\sum_i \frac{J_{\eta i}^{ab}}{J_{\eta\eta^*}^a}\exp(ik_i^b b)\beta_i\right.$$

$$+ \sum_{\xi^*} \frac{J_{\eta\xi^*}^{ab}}{J_{\eta\eta^*}^a}\exp(ik_{\xi^*}^b b)\beta_{\xi^*}$$

$$+ \left.\sum_\xi \frac{J_{\eta\xi}^{ab}}{J_{\eta\eta^*}^a}\beta_\xi\right], \quad\quad\text{(A4b)}$$

and

$$\alpha_\eta\exp[iQ(a+b)] = \sum_i \frac{J_{\eta^*i}^{ab}}{J_{\eta^*\eta}^a}\exp(ik_i^b b)\beta_i$$

$$+ \sum_{\xi^*} \frac{J_{\eta^*\xi^*}^{ab}}{J_{\eta^*\eta}^a}\exp(ik_{\xi^*}^b b)\beta_{\xi^*}$$

$$+ \sum_\xi \frac{J_{\eta^*\xi}^{ab}}{J_{\eta^*\eta}^a}\beta_\eta. \quad\quad\text{(A4c)}$$

Dropping exponentially small terms gives

$$\alpha_j\exp[iQ(a+b)] = \sum_i \exp(ik_j^a a)\frac{J_{j^*i}^{ab}}{J_{j^*j}^a}\exp(ik_i^b b)\beta_i$$

$$+ \sum_\xi \exp(ik_j^a a)\frac{J_{j^*\xi}^{ab}}{J_{j^*j}^a}\beta_\xi, \quad\text{(A5a)}$$

$$0 = \sum_i \frac{J_{\eta i}^{ab}}{J_{\eta\eta^*}^a}\exp(ik_i^b b)\beta_i + \sum_\xi \frac{J_{\eta\xi}^{ab}}{J_{\eta\eta^*}^a}\beta_\xi, \quad\text{(A5b)}$$

and

$$\alpha_\eta\exp[iQ(a+b)] = \sum_i \frac{J_{\eta^*i}^{ab}}{J_{\eta^*\eta}^a}\exp(ik_i^b b)\beta_i + \sum_\xi \frac{J_{\eta^*\xi}^{ab}}{J_{\eta^*\eta}^a}\beta_\eta.$$

$$\text{(A5c)}$$

There are four equations, like Eq. (A5b), which have a zero on the left-hand side. These equations are solved for the amplitudes of the large-$|\text{Im}[k]|$ states labeled by ξ, ξ^*, η, and η^* in terms of amplitudes of small-$|\text{Im}[k]|$ states labeled by i and j. One easily verifies that there are enough conditions to do this. One then eliminates the amplitudes β_i (say) and derives an eigenvalue equation for the amplitudes α_j. This equation does not contain exponentially large (or small) factors and can be handled without numerical difficulty.

The procedure described above is generally applicable. It is somewhat easier to apply if the number of large-$|\text{Im}[k]|$ states is the same in each material. Thus the number of ξ's and the number of η's is the same and Eq. (A5b) can be directly solved for β_ξ in terms of the β_i's. (In general, these four equations must be combined and solved together.) Inspection of Fig. 5, which shows complex band structure for typical cases, reveals that it is usu-

ally possible to choose γ and γ' in Eqs. (A2) such that the number of η's and ξ's is the same.

For the case where the number of η's and ξ's is the same, one can easily derive a closed-form expression for the matrix M in the superlattice eigenvalue equation [Eqs. (3)]. The result is somewhat complicated and will not be given here. However, for many cases, the coupling between the small-$|\operatorname{Im}[k]|$ states and the large-$|\operatorname{Im}[k]|$ states, given by factors like $J^{ab}_{j*_{\eta}}/J^{a}_{j*_{j}}$, are quite small. Treating such factors as small parameters and calculating to second order in these small parameters (the next term is fourth order) gives the M matrix as

$$
M_{jj'} = \sum_i \exp(ik_j^a a) \left[\frac{J^{ab}_{j*i}}{J^{a}_{j*j}} \exp(ik_i^b b) \frac{J^{ba}_{i*j'}}{J^{b}_{i*i}} - \sum_{\xi,\eta^*} \frac{J^{ab}_{j*i}}{J^{a}_{j*j}} \frac{\exp(ik_i^b b)J^{ba}_{i*\eta^*}}{J^{b}_{i*i}} \frac{J^{ab}_{\eta\xi}}{J^{a}_{\eta\eta^*}} \frac{J^{ba}_{\xi*j'}}{J^{b}_{\xi*\xi}} \right.
$$
$$
\left. - \sum_{\xi,\eta^*} \frac{J^{ab}_{j*\xi}}{J^{a}_{j*j}} \frac{J^{ba}_{\xi*\eta^*}}{J^{b}_{\xi*\xi}} \frac{J^{ab}_{\eta i}}{J^{a}_{\eta\eta^*}} \frac{\exp(ik_i^b b)J^{ba}_{i*j'}}{J^{b}_{i*i}} \right] . \tag{A6}
$$

If one considers the four bands which appear in the 16-band model and not in the 12-band model as large-$|\operatorname{Im}[k]|$ bands in the above sense, the second and third terms on the right-hand side of Eq. (A6) give the contribution of these bands to the superlattice. Both of these terms are second order in the small coupling parameter. The square of this small coupling parameter is found to be numerically of order 10^{-6}. Therefore these bands make essentially no contribution to the superlattice states. This result justifies the use of the 12-band model. It also justifies calculating bulk states in the 16-band model [i.e., using Eq. (10) of paper I] and simply disregarding the four large-$|\operatorname{Im}[k]|$ states [i.e., dropping the second and third terms on the right-hand side of Eq. (A6)]. Indeed, these two approaches give virtually identical results.

[1]For a recent review, see *Proceedings of the NATO Advanced Study Institute on Molecular Beam Epitaxy and Heterostructures, Erice, 1983*, edited by L. L. Change and K. Ploog (Nijhoff, Leyden, 1985).

[2]N. Holonyak, Jr., R. M. Kolbas, R. D. Dupuis, and P. D. Dapkus, IEEE J. Quantum Electron. **QE-16**, 170 (1980).

[3]D. L. Smith, T. C. McGill, and J. N. Schulman, App. Phys. Lett. **43**, 180 (1983).

[4]M. Heiblum, Solid-State Electron. **24**, 343 (1981).

[5]F. Capasso and R. A. Kiehl, J. Appl. Phys. **58**, 1366 (1985).

[6]D. L. Smith and C. Mailhiot, Phys. Rev. B **33-I**, 8345 (1986).

[7]R. People, K. W. Wecht, K. Alavi, and A. Y. Cho, App. Phys. Lett. **43**, 118 (1983).

[8]F. Capasso, K. Mohammed, A. Y. Cho, R. Hull, and A. L. Hutchinson, App. Phys. Lett. **47**, 420 (1985).

[9]F. Capasso, K. Mohammed, A. Y. Cho, R. Hull, and A. L. Hutchinson, Phys. Rev. Lett. **55**, 1152 (1985).

[10]K. Shum, P. P. Ho, R. R. Alfano, D. F. Welch, G. W. Wicks, and L. F. Eastman, Phys. Rev. B **32**, 3806 (1985).

[11]W. Stolz, L. Tapfer, A. Breitschwerdt, and K. Ploog, Appl. Phys. A **38**, 97 (1985).

[12]J. S. Weiner, D. S. Chemla, D. A. B. Miller, T. H. Wood, D. Sivco, and A. Y. Cho, App. Phys. Lett. **46**, 619 (1985).

[13]G. Bastard, Phys. Rev. B **24**, 5693 (1981).

[14]G. Bastard, Phys. Rev. B **25**, 7584 (1982).

[15]S. R. White and L. J. Sham, Phys. Rev. Lett. **47**, 879 (1981).

[16]M. Altarelli, Phys. Rev. B **28**, 842 (1983).

[17]C. Mailhiot, D. L. Smith, and T. C. McGill, J. Vac. Sci. Technol. B **2**, 371 (1984).

[18]M. L. Cohen and T. K. Bergstresser, Phys. Rev. **141**, 789 (1966).

[19]A. N. Pikhtin, Fiz. Tekh. Poluprovdn. **11**, 425 (1977) [Sov. Phys.—Semicond. **11**, 245 (1977)].

[20]E. Hess, I. Topol, K.-R. Schulze, H. Neumann, and K. Unger, Phys. Status Solidi B **55**, 187 (1973).

[21]G. F. Koster, J. O. Dimmock, R. G. Wheeler, and H. Statz, *Properties of the Thirty-two Point Groups* (MIT Press, Cambridge, Mass., 1963).

[22]P. O. Löwdin, J. Chem. Phys. **19**, 1396 (1951).

[23]E. O. Kane, in *Physics of III-V Compounds*, edited by R. K. Williamson and A. C. Beer (Academic, New York, 1966), Vol. 1, p. 75.

[24]H. Mathieu, P. Merle, E. L. Ameziane, B. Archilla, and J. Camassel, Phys. Rev. B **19**, 2209 (1979).

[25]R. M. Martin, Phys. Rev. B **1**, 4005 (1970).

[26]G. D. Pitt, Contemp. Phys. **18**, 137 (1977).

[27]P. Lawaetz, Phys. Rev. B **4**, 3460 (1971).

[28]In optical measurements, the deformation potential c and the combination $l+2m$ cannot be separately determined. Separately specifying these numbers is equivalent to specifying a stress dependence of the energy zero. For a single material, such a specification has no physical significance. For a heterojunction system, separately specifying the deformation potentials in each material specifies the stress dependence of the overall energy zero (no physical significance) and the stress dependence of the valence-band offset. There is virtually no information available on the stress dependence of valence-band offsets and we have therefore adopted a reasonable, but arbitrary, prescription.

[29]L. Esaki and R. Tsu, IBM J. Res. Dev. **14**, 61 (1970).

[30]See, for examle, J. N. Schulman and T. C. McGill, in *Synthetic Modulated Structure Materials*, edited by L. L. Chang and B. C. Giessen (Academic, New York, 1985).

[31]The twofold degeneracy is ensured by time-reversal symmetry.

[32]R. C. Miller, D. A. Kleinman, and A. C. Gossard, Phys. Rev. B 29, 7085 (1984).

[33]J. N. Schulman and Y.-C. Chang, Phys. Rev. B 31, 2056 (1985).

[34]Y.-C. Chang and J. N. Schulman, Phys. Rev. B 31, 2069 (1985).

[35]G. D. Sanders and Y.-C. Chang, Phys. Rev. B 31, 6892 (1985).

[36]A. Fasolino and M. Altarelli, in Two-Dimensional Systems, Heterostructures, and Superlattices, edited by G. Bauer, F. Kuchar, and H. Heinrich (Springer-Verlag, Berlin, 1984), p. 176.

[37]M. Altarelli, U. Ekenberg, and A. Fasolino, Phys. Rev. B 32, 5138 (1985).

[38]S. S. Nedorezov, Fiz. Tverd. Tela (Leningrad) 12, 2269 (1970) [Sov. Phys.—Solid State 12, 1814 (1971)].

[39]See Eqs. (43) and (44) of paper I.

[40]As in paper I, we use $|s\rangle$ to represent the Γ_1 conduction-band state and $|x\rangle, |y\rangle, |z\rangle$ to represent the Γ_{15} valence-band states of the reference Hamiltonian.

[41]However, because the difference between the 16- and 12-band models are numerically very slight, we expect that the envelope-function continuity should be very nearly satisfied in the 12-band model.

[42]J. W. Matthews and A. E. Blakeslee, J. Cryst. Growth 27, 118 (1974); 29, 273 (1975).

[43]G. C. Osbourn, J. Appl. Phys. 53, 1586 (1982); J. Vac. Sci. Technol. 21, 469 (1982); Phys. Rev. B 27, 5126 (1983); J. Vac. Sci. Technol. A 3, 826 (1985).

[44]J. E. Schirber, I. J. Fritz, and L. R. Dawson, App. Phys. Lett. 46, 187 (1985).

[45]Consistency constraints are given in paper I, in particular, see Eq. (31).